

MIT Open Access Articles

Sustained antigen availability during germinal center initiation enhances antibody responses to vaccination

The MIT Faculty has made this article openly available. **Please share** how this access benefits you. Your story matters.

Citation: Tam, Hok Hei et al. "Sustained Antigen Availability during Germinal Center Initiation Enhances Antibody Responses to Vaccination." Proceedings of the National Academy of Sciences 113.43 (2016): E6639–E6648. © 2017 National Academy of Sciences

As Published: <http://dx.doi.org/10.1073/pnas.1606050113>

Publisher: National Academy of Sciences (U.S.)

Persistent URL: <http://hdl.handle.net/1721.1/108787>

Version: Final published version: final published article, as it appeared in a journal, conference proceedings, or other formally published context

Terms of Use: Article is made available in accordance with the publisher's policy and may be subject to US copyright law. Please refer to the publisher's site for terms of use.



Sustained antigen availability during germinal center initiation enhances antibody responses to vaccination

Hok Hei Tam^{a,b,1}, Mariane B. Melo^{b,c,1}, Myungsun Kang^{a,d,1}, Jeisa M. Pelet^b, Vera M. Ruda^b, Maria H. Foley^b, Joyce K. Hu^e, Sudha Kumari^{b,c}, Jordan Crampton^e, Alexis D. Baldeon^b, Rogier W. Sanders^{f,g}, John P. Moore^f, Shane Crotty^{e,h,i}, Robert Langer^{a,b,d}, Daniel G. Anderson^{a,b,d,2,3}, Arup K. Chakraborty^{a,c,d,j,k,l,2,3}, and Darrell J. Irvine^{b,c,h,k,m,2,3}

^aDepartment of Chemical Engineering, Massachusetts Institute of Technology, Cambridge, MA 02139; ^bDavid H. Koch Institute for Integrative Cancer Research, Massachusetts Institute of Technology, Cambridge, MA 02139; ^cRagon Institute of Massachusetts General Hospital, Massachusetts Institute of Technology, & Harvard, Cambridge, MA 02139; ^dInstitute for Medical Engineering & Science, Massachusetts Institute of Technology, Cambridge, MA 02139; ^eDivision of Vaccine Discovery, La Jolla Institute for Allergy & Immunology, La Jolla, CA 92037; ^fDepartment of Microbiology and Immunology, Weill Medical College of Cornell University, New York, NY 10021; ^gDepartment of Medical Microbiology, Academic Medical Center, University of Amsterdam, 1105 AZ Amsterdam-Zuidoost, The Netherlands; ^hCenter for HIV/AIDS Vaccine Immunology and Immunogen Discovery, La Jolla, CA 92037; ⁱDepartment of Medicine, University of California, San Diego School of Medicine, La Jolla, CA 92037; ^jDepartment of Physics, Massachusetts Institute of Technology, Cambridge, MA 02139; ^kDepartment of Biological Engineering, Massachusetts Institute of Technology, Cambridge, MA 02139; ^lDepartment of Chemistry, Massachusetts Institute of Technology, Cambridge, MA 02139; and ^mHoward Hughes Medical Institute, Chevy Chase, MD 20815

Edited by Philippa Marrack, Howard Hughes Medical Institute, National Jewish Health, Denver, CO, and approved August 19, 2016 (received for review April 14, 2016)

Natural infections expose the immune system to escalating antigen and inflammation over days to weeks, whereas nonlive vaccines are single bolus events. We explored whether the immune system responds optimally to antigen kinetics most similar to replicating infections, rather than a bolus dose. Using HIV antigens, we found that administering a given total dose of antigen and adjuvant over 1–2 wk through repeated injections or osmotic pumps enhanced humoral responses, with exponentially increasing (exp-inc) dosing profiles eliciting >10-fold increases in antibody production relative to bolus vaccination post prime. Computational modeling of the germinal center response suggested that antigen availability as higher-affinity antibodies evolve enhances antigen capture in lymph nodes. Consistent with these predictions, we found that exp-inc dosing led to prolonged antigen retention in lymph nodes and increased Tfh cell and germinal center B-cell numbers. Thus, regulating the antigen and adjuvant kinetics may enable increased vaccine potency.

vaccination kinetics | antigen retention | humoral response | computational immunology | germinal center formation

Subunit vaccines based on recombinant protein antigens combined with adjuvants can safely elicit protective humoral immune responses in humans, and they have become a cornerstone of modern public health (1, 2). Recent advances in structure-based vaccine design (3, 4) and progress in the development of adjuvants that are safe and effective for prophylactic vaccines (5) have helped drive the field. However, several challenges remain: A number of protein vaccines, such as candidate vaccines against HIV and malaria, have tended to elicit short-lived immunity (6, 7). In HIV, broadly neutralizing antibodies (BNABs) isolated from infected patients are generally characterized by high degrees of somatic hypermutation (SHM) (8), but methods to generate such highly mutated antibodies by vaccination remain unknown. SHM occurs in germinal centers (GCs) within lymphoid organs, and data from animal models demonstrate a critical role for follicular helper T cells in the induction of GCs and promotion of affinity maturation (9, 10). To date, methods to promote Tfh generation and long-lived germinal centers during vaccination remain unclear (11–15). Much attention has focused on the use of adjuvants to promote affinity maturation, but it remains unclear if adjuvants alone can provide the necessary immunological driving forces for promoting extensive affinity maturation (16).

During acute infections, which often provoke robust germinal center responses and durable humoral immunity, microorganism replication typically occurs over the course of one to several weeks (17–19). During this time, recognition of molecular danger

signals contained within the pathogen sustains stimulation of the innate immune system, and a continuous supply of antigen is provided to the adaptive immune system. In contrast to these patterns of antigen and inflammatory cues during infection, typical subunit vaccines show much more rapid clearance following injection. During a primary immune response, parenterally injected proteins are detected in lymph nodes within minutes to a few hours but are largely flushed away within 1–2 d (12, 20). Adjuvants such as alum and MF59 are believed to act as antigen depots altering these kinetics, but biodistribution studies suggest that clearance of antigen from injection sites and lymph nodes is often nearly indistinguishable for soluble vs. alum-adsorbed or MF59-adjuvanted antigens (21–23). As such, the effect of subunit vaccine kinetics on the humoral immune response remains poorly understood. Given that germinal centers peak multiple weeks after antigen exposure, it is reasonable to postulate that antigen kinetics may have a profound effect on the magnitude

Significance

We explored the effect of nontraditional vaccine dosing profiles on antibody titers of vaccines and discovered that certain dosing profiles demonstrate >10-fold higher antibody production than the traditional single-dose prime–boost method. We also present a computational model that captures the experimental results and provides a mechanistic understanding of the biology behind the effectiveness of our strategy. This work has clinical significance in vaccine design because it is a simple method to increase the efficacy of subunit vaccines, which may lead to the development of efficacious vaccines for diseases such as HIV.

Author contributions: H.H.T., M.B.M., M.K., J.M.P., V.M.R., M.H.F., J.K.H., S.C., R.L., D.G.A., A.K.C., and D.J.I. designed research; H.H.T., M.B.M., M.K., J.M.P., V.M.R., M.H.F., J.K.H., S.K., J.C., and A.D.B. performed research; H.H.T., M.B.M., M.K., J.M.P., V.M.R., M.H.F., J.K.H., S.K., R.W.S., J.P.M., S.C., D.G.A., A.K.C., and D.J.I. contributed new reagents/analytic tools; H.H.T., M.B.M., M.K., J.M.P., V.M.R., M.H.F., J.K.H., S.K., D.G.A., A.K.C., and D.J.I. analyzed data; and H.H.T., M.B.M., M.K., J.M.P., V.M.R., M.H.F., R.L., D.G.A., A.K.C., and D.J.I. wrote the paper.

The authors declare no conflict of interest.

This article is a PNAS Direct Submission.

¹H.H.T., M.B.M., and M.K. contributed equally to this work.

²D.G.A., A.K.C., and D.J.I. contributed equally to this work.

³To whom correspondence may be addressed. Email: djirvine@mit.edu, dgander@mit.edu, or arupc@mit.edu.

This article contains supporting information online at www.pnas.org/lookup/suppl/doi:10.1073/pnas.1606050113/-DCSupplemental.

Here we explored the effects of systematically varied temporal dosing patterns on the humoral immune response to model HIV subunit vaccines consisting of recombinant CD4 binding site-presenting gp120 monomer (24, 25) or SOSIP native-like HIV Env trimer proteins (26–28). We find that certain extended-duration dosing profiles increased the strength of the humoral response, with exponentially increasing patterns providing the greatest enhancement. Guided by a computational model of the effects of vaccine kinetics on the germinal center response, we found that exponentially increasing dosing kinetics promoted capture and retention of the antigen in lymph nodes, leading to increased germinal center B-cell expansion, plasma cell generation, and Tfh cell numbers.

Results

Exponentially Increasing Dosing Profiles During Priming Durably Increase the Production of Antigen-Specific IgG. We hypothesized that extended exposure to antigen and adjuvant, better mimicking the kinetics of live infections, would augment the response to vaccination. As a model vaccine, we used a previously described gp120 stripped core antigen containing the CD4 binding site (24, 25), which was mixed with monophosphoryl lipid A (MPLA) as a clinically relevant adjuvant (29). We first evaluated the effect of altering vaccination kinetics by extending the dosing of the prime over 1 wk. Groups of mice were immunized with either a conventional bolus injection on day 0 or seven daily injections over 1 wk testing three concepts: exponentially increasing (exp-inc), exponentially decreasing (exp-dec), or constant dosing, where the summed total dose of antigen and adjuvant was kept the same in all groups (Fig. 1A and Table S1). All groups received a boost as a single bolus injection at day 21. Following priming, exp-inc and constant dosing profiles elicited strikingly higher IgG responses by day 14 compared with bolus immunization, with anti-gp120 Ab concentrations 14-fold and ~8-fold higher ($P < 0.001$), respectively, than bolus injection at day 14, roughly equivalent to the titers achieved by traditional

bolus immunization after the boost (Fig. 1 *B* and *C*). By contrast, an exp-dec dosing pattern elicited titers postprime that were indistinguishable from the bolus control. Following the boost administered at day 21, animals that received an exp-inc prime continued to show higher anti-gp120 Ab levels, which were 2.7 times greater (average over time) than the bolus-primed group (Fig. 1*C*; $P < 0.001$). This effect was durable, lasting 150 d. By contrast, the constant-dosing prime elicited Ab levels only 1.6 times higher than bolus injection ($P = 0.040$), and the exp-dec prime was not significantly different from bolus prime. Thus, certain extended vaccine kinetic profiles, especially in an increasing dosing pattern, enhanced the long-term concentration of antigen-specific IgG produced.

Extended Dosing Profiles over 2 wk Maximize Antibody Titers. We hypothesized that dosing over a 1-wk period may be suboptimal, given the more prolonged kinetics of germinal centers and the kinetics of many acute infections. As exp-inc dosing resulted in elevated antibody titers, we next tested how the duration of this dosing pattern influenced the humoral response. We compared exp-inc dosing profiles administered over 7, 14, or 21 d, keeping the total number of injections (7) and total dose constant. For each pattern, the bolus boost was given 14 d after the last priming injection (Fig. 2A and Fig. S1A). To account for the effect of a later boost, we also introduced a second control with single-dose prime and a boost at day 28. As seen in Fig. 2B, extending the dosing course from 7 to 14 d increased the magnitude of the antibody response, with the 2-wk exp-inc dosing pattern eliciting ~48-fold higher concentrations of gp120-specific antibodies than the corresponding bolus prime group by day 21 ($P < 0.001$; Fig. 2B). Further extending the exp-inc dosing profile from 14 to 21 d led to a slightly weaker humoral response than the 2-wk profile (Fig. S1). Postboost, 1- and 2-wk exp-inc dosing elicited sustained gp120-specific IgG levels that were 3.6-fold ($P < 0.001$) and 6.6-fold higher ($P < 0.001$) than their equivalently timed bolus prime/boost controls (Fig. 2C).

To determine the relative importance of an increasing dosing profile on the prime vs. boost response, we compared exp-inc dosing profiles administered only during the prime, only during

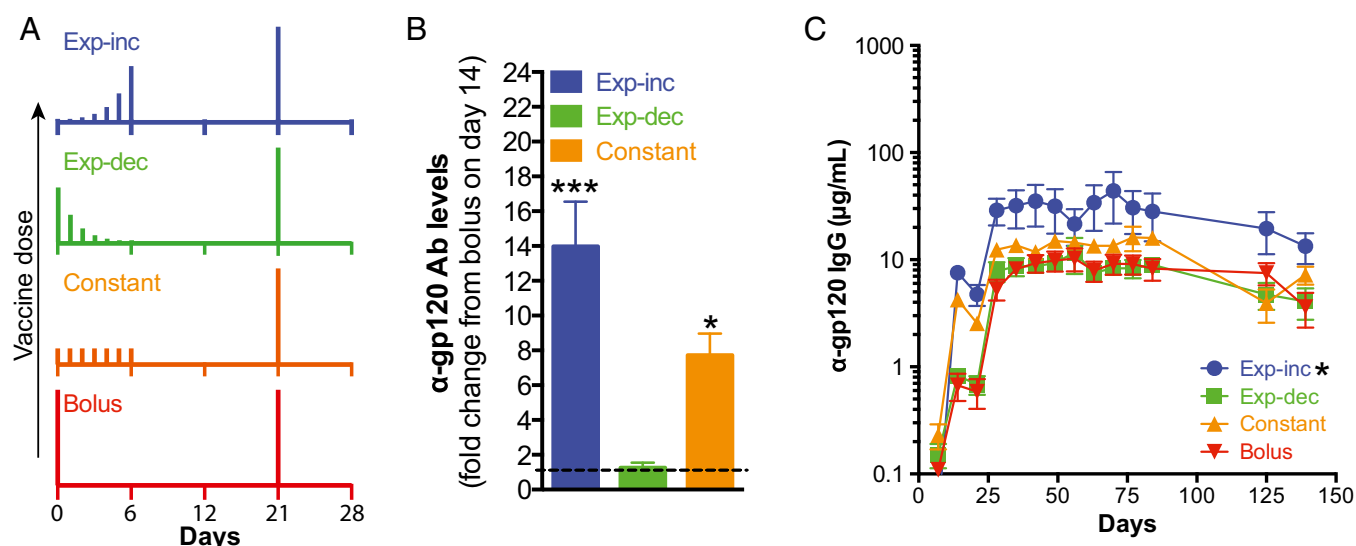


Fig. 1. Exponentially increasing dosing schedules during priming durably increase antigen-specific IgG production relative to traditional bolus immunization. Groups of C57BL/6 mice ($n = 5$ per group) were immunized with 5 μ g gp120 mixed with 25 μ g MPLA according to the dosing schedules shown in A, followed by a single bolus booster injection of 5 μ g gp120 + 25 μ g MPLA on day 21. (B) Fold change in antibody concentration on day 14 postprime relative to bolus injection. * $P < 0.05$; *** $P < 0.0001$ compared with bolus injection determined by ANOVA with Dunnett's test post hoc using bolus injection as the control. Shown are means \pm SEM. (C) Total serum anti-gp120 IgG as measured by ELISA. Asterisk indicates statistically different from boost d21 group as determined by two-way ANOVA with Dunnett's post hoc test using bolus injection as the control. Data are representative of two independent experiments.

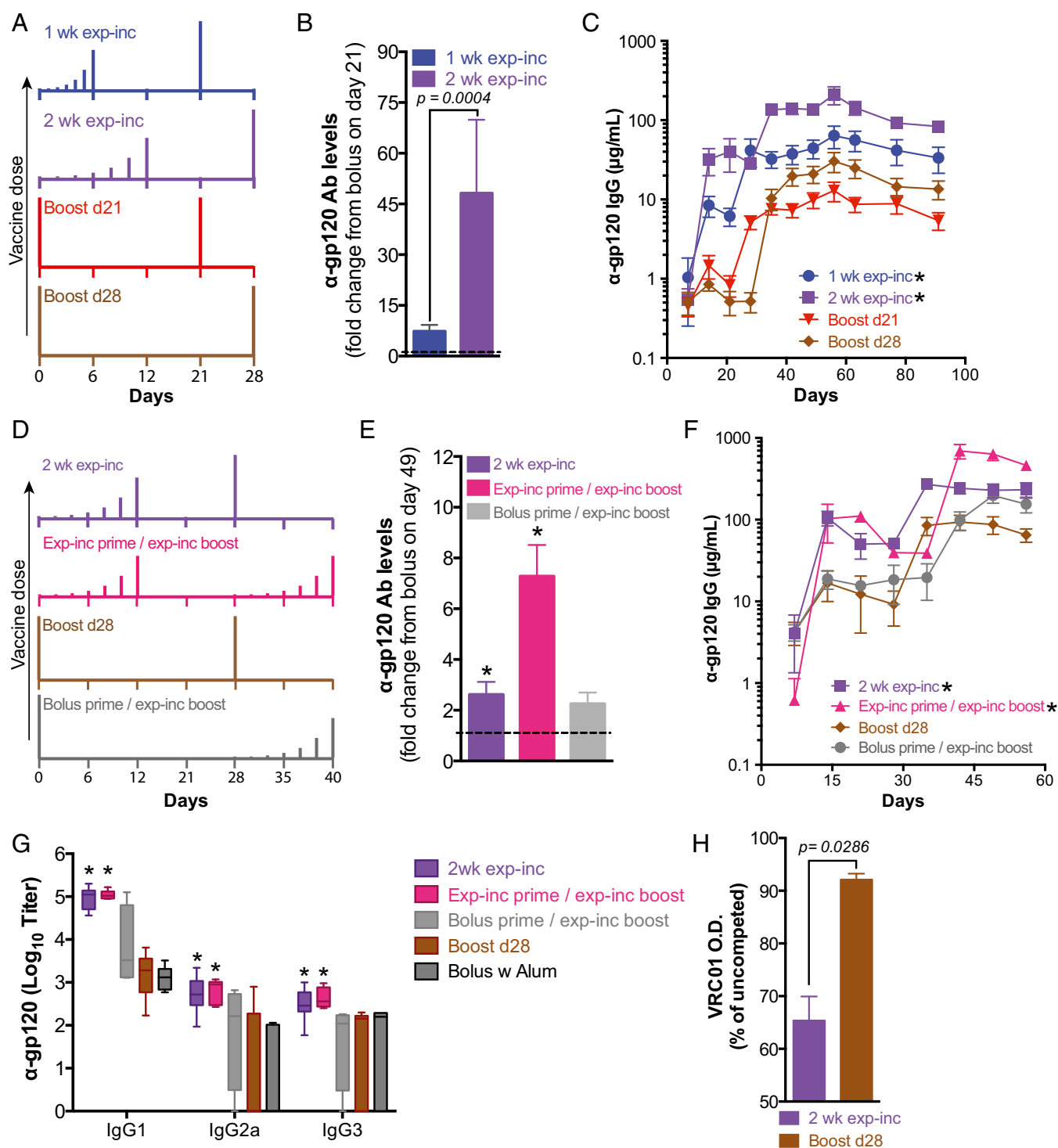


Fig. 2. Exponentially increasing dosing profiles extended over 2 wk with an exponentially increasing boost enhance the humoral response. Groups of C57BL/6 mice were immunized with 5 μ g gp120 + 25 μ g MPLA following the dosing schedules shown in **A** and **D**. (**B**) Fold change in antibody concentration on day 21 postprime relative to bolus injection. p was determined by unpaired Mann–Whitney test. (**C**) Total serum anti-gp120 IgG ($n = 10$ per group) as measured by ELISA. Asterisk indicates statistically different from boost d21 group as determined by two-way ANOVA with Dunnett's post hoc test using bolus injection as the control. (**E**) Fold change in antibody concentration on day 49 (postboost) relative to bolus injection. * $P < 0.05$ determined by Kruskal–Wallis test with Dunn's multiple comparison's test. (**F**) Total serum IgG ($n = 5$ per group) measured by ELISA. Asterisk indicates statistically different from boost d21 group as determined by two-way ANOVA with Dunnett's post hoc test using bolus injection as the control. (**G**) Mice were immunized either with gp120 plus MPLA following schedules shown in **D** or with gp120 formulated in 100 μ g alum (aluminum phosphate, prime day 0, boost day 28). Serum was collected at day 49, and anti-gp120 isotype titers were analyzed by ELISA. Asterisk indicates statistically different from boost d28 group as determined by two-way ANOVA with Dunnett's post hoc test using bolus injection as the control. (**H**) ELISA for binding to gp120 for day 49 sera was performed in the presence of competing broadly neutralizing antibody VRC01. Shown is ELISA optical density as a percentage of uncompleted signal. p was calculated by unpaired Mann–Whitney test. All values shown are mean \pm SEM. Data are representative of experiments done twice (**A–C**) or once (**D–H**), using at least five mice per group.

the boost, or during both prime and boost (Fig. 2D). Incorporation of an exp-inc dosing profile for both the prime and boost resulted in significantly higher serum Ab concentrations than either exp-inc prime/bolus boost or bolus prime/exp-inc boost regimens (Fig. 2E and F). To evaluate the effect of extended dosing on class switching, we analyzed titers of different Ab isotypes induced. Exp-inc dosing substantially increased the titers of multiple Ig isotypes, including IgG1, IgG3, and IgG2a that was near background following traditional bolus immunization (Fig. 2G). We also compared exp-inc vaccination to traditional bolus vaccination using alum as the most common clinical adjuvant, which has been proposed to provide a depot effect with some antigens (30). As shown in Fig. S2, alum provided comparable antibody responses to bolus vaccination using MPLA as adjuvant ($P = 0.88$), but was much inferior to exp-inc dosing of the vaccine, and also elicited almost exclusively IgG1 titers ($P = 0.038$; Fig. 2G). Finally, we tested the capacity of vaccine-elicited antibodies to compete with the BNAbs VRC01 for binding to the gp120 antigen by ELISA; exp-inc vaccine dosing increased the proportion of antibodies induced that blocked VRC01 binding (Fig. 2H). Altogether, these results indicate that for a given total quantity of antigen and adjuvant, extended vaccine kinetics obtained by administering the vaccine over at least 2 wk in increasing doses is capable of durably increasing total output serum concentrations of elicited antigen-specific IgG by more than sevenfold, elevating the production of multiple isotypes of Ab.

A Computational Model of the Germinal Center Response Predicts Antibody-Based Feedback Governs the Response to Extended Dosing Vaccines. In a traditional bolus immunization, the half-life of the antigen present in lymph nodes is shorter than the time scale over which GC reactions start producing higher affinity IgG antibodies relative to the initial IgM response (12, 20). Thus,

most antigen displayed on follicular dendritic cells (FDCs) is in the form of immune complexes (IC) of antigen with weakly bound IgM antibodies (31, 32); this may lead to a suboptimal level of antigen concentration on FDCs. We hypothesized that extended vaccine dosing may better match the time scale of antigen availability to the kinetics of the GC reaction compared with bolus immunization, leading to more ICs formed with newly evolved higher-affinity antibodies, thereby promoting more prolonged retention on FDCs. To explore whether this feedback mechanism alone can account for the significant effect of extended dosing profiles observed experimentally, we constructed a coarse-grained computational model with a minimal number of parameters. The goal of the model was to test whether our hypothesis could provide an explanation for the data and, if so, to subject it to experimental tests. The model particularly focuses on antigen transport, the GC reaction, and antibody production by plasma cells in a lymph node (Fig. 3A). It makes the following assumptions: (i) As a simplified approximation of experimental observations of soluble antigen transport following injection, we assume that antigen arrives at the lymph node immediately following immunization, and free antigen in the lymph node clears exponentially over time with a half-life of ~ 17 h (20, 33). Natural IgM initiates the immune response and captures antigen arriving in the lymph node with a low affinity (32). (ii) B cells class-switch only to IgG and not to other Ig subclasses after the GC reaction ensues. (iii) The onset of IgG production occurs 6 d after the initial antigen injection, reflecting the observation that it takes a few days for GC reactions to occur before class switching initiates (34, 35). (iv) The GC B-cell population size is assumed to be constant during the GC reaction. Although this is incorrect, qualitative results emerging from models of evolutionary processes that make this approximation are often accurate (36). (v) The formation of ICs is the rate-limiting step in antigen presentation to GC B cells; that is, the model assumes that transport

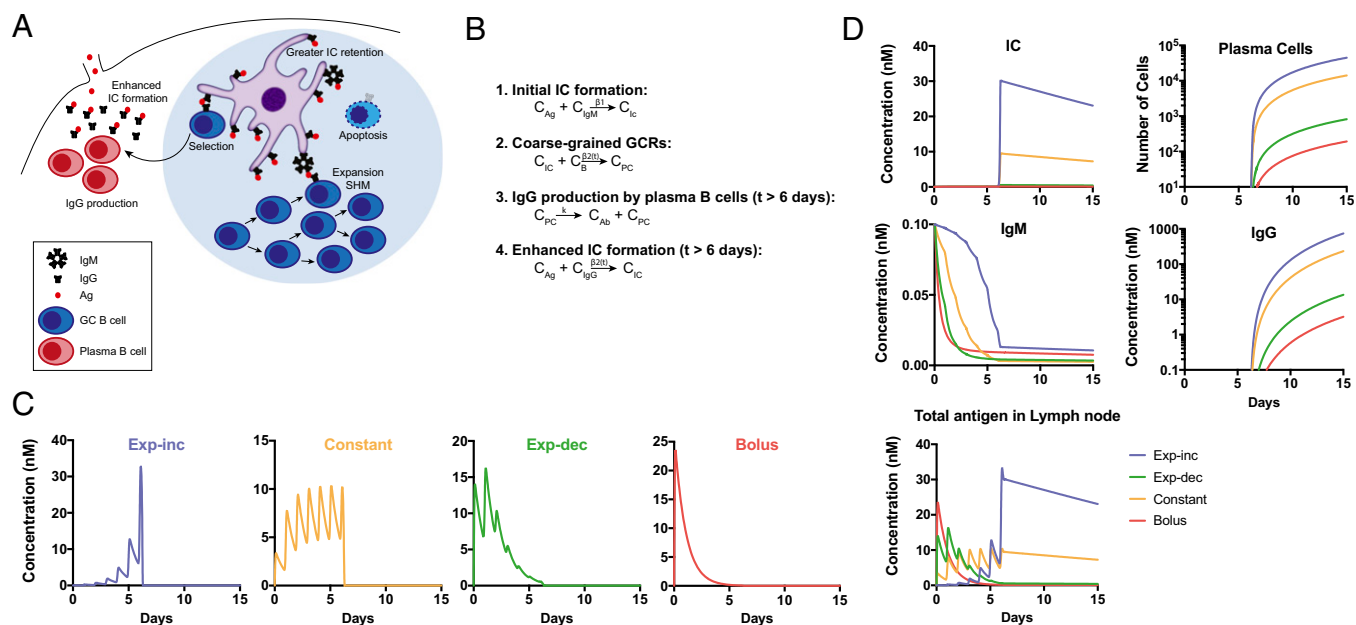


Fig. 3. A computational model of the germinal center response predicts enhanced immune complex formation and IgG production by extended-dosing/increasing vaccination profiles. (A) Schematic of components of antigen transport, GC reaction, and antibody production model. (B) Four reactions of the model including antigen capture by ICs at initial and later stages of the immune response, coarse-grained germinal center reaction, and antibody production. C_B , concentration of germinal center B cells; C_{Ag} , concentration of free Ag; C_{IC} , concentration of ICs; C_{IgM} , concentration of IgM; C_{IgG} , concentration of IgG; C_{PC} , concentration of plasma cells. (C) Kinetic profile of free antigen in lymph nodes predicted by the model with fitted k (2.56×10^6 antibodies per plasma cell per day). (D) Kinetic profiles of IC, IgM, IgG, plasma cells, and total antigen in lymph node (free Ag + IC) predicted by the model. See also *Germinal Center Model Calculations in Materials and Methods* and [Table S3](#) for mathematical representation of the model.

of immune complexes to FDCs is relatively fast. (vi) Ten percent of selected B cells differentiate to plasma cells (24). (vii) IgG affinity evolves linearly and increases by 100-fold by the end of the GC reaction (24). Based on these assumptions, four key reactions summarize the model (Fig. 3B). During the early phase of the immune response, free antigen is captured by IgM at a slow rate (proxy for affinity), β_1 (Reaction 1). B cells bind to ICs in GCs with an increasing rate β_2 (proxy for affinity) as a function of time and become plasma cells (Reaction 2), which ultimately leads to production of IgG (Reaction 3). Because this is a coarse-grained model, we consider only the average affinity of IgGs, although in reality, there is a heterogeneous distribution. Plasma cells derived from the GC reaction produce antibodies at a rate k (Reaction 3), and the resulting higher-affinity antibodies capture antigen (Reaction 4) at a rate β_2 . Parameter values were taken from the literature (Table S2) when available, except for k , which is the number of antibodies produced by each plasma cell per day. Nonlinear regression fitting of the model antibody output to IgG concentrations measured experimentally at days 7 and 14 following gp120 immunizations was performed to determine the best value of k . This yielded a value for k of 2.56×10^6 antibodies per plasma cell

per day, which is in rough agreement with the reported rate of $\sim 10^7$ IgG molecules secreted by a single plasma cell per day (37).

Using these parameters, we modeled the GC reaction, immune complex formation, and IgG production for each of the 1-wk vaccine dosing schedules studied experimentally in Fig. 1 (Fig. 3C). As shown in Fig. 3D, the model predicts that the hierarchy of antibody production among the different dosing schemes mirrors the hierarchy of IC concentrations. Exp-inc dosing produces the highest level of immune complex formation and thus the highest level of antibody output. The exp-inc dosing profile also leads to increased GC activity and increased numbers of plasma cells. By contrast, the calculations suggest that IC accumulation using the exp-dec dosing scheme is very low and similar to that from a bolus immunization (Fig. 3D), consistent with the experimental finding that antibody production in these two cases was similar. A key prediction of the model is that total antigen in lymph nodes quickly decays 24 h after the bolus immunization, whereas antigen is retained at high levels for many days at the end of the exp-inc dosing schedule (Fig. 3D). Thus, a simple model of the GC reaction focused on the effect of early antibody evolution on antigen capture in ICs reproduces the

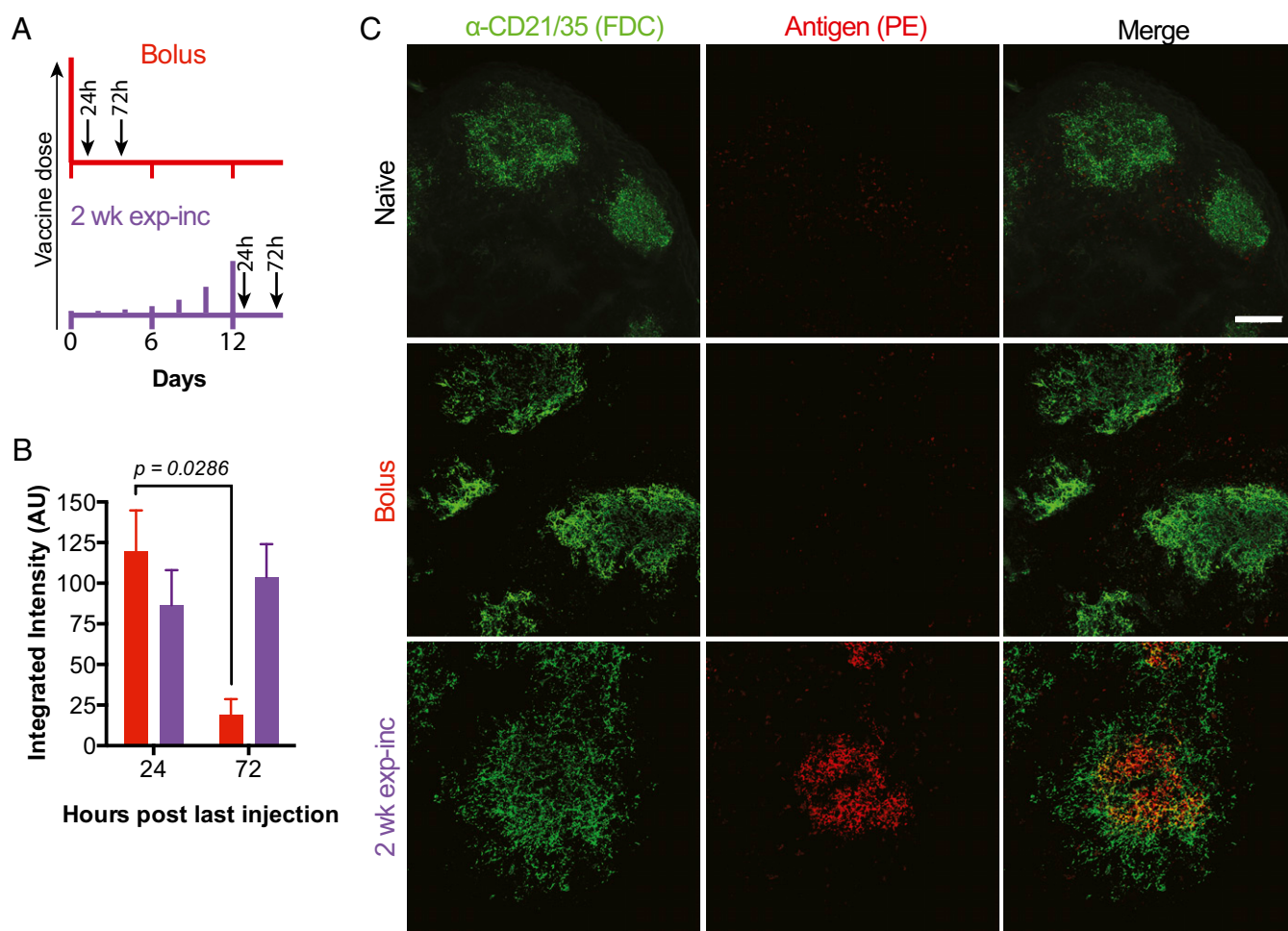


Fig. 4. Exponentially increasing vaccine dosing leads to enhanced antigen capture and retention in draining lymph nodes. Groups of albino C57BL/6 mice received s.c. injections of 5 μ g of IRDye800-labeled gp120 plus 25 μ g of MPLA. Relative amounts of gp120 in the lymph nodes were quantified by fluorescence. (A) Dosing and sampling profiles used in this experiment. (B) Fluorescence detected from lymph nodes ex vivo ($n = 4$ per group) at 24 or 72 h post-last injection. P value was calculated by unpaired Mann–Whitney test. Data are representative of two independent experiments. (C) Groups of C57BL/6 mice ($n = 2$ per group) were vaccinated with 5 μ g phycoerythrin and 25 μ g MPLA by bolus or exp-inc dosing following the schedule in A, followed by collection of lymph nodes for imaging at 72 h after bolus or after last injection of 2 wk exp-inc dosing. FDC networks were labeled in situ by i.p. injection of anti-CD21/35 antibody 16 h before tissue collection. Collected tissues were clarified and imaged intact by confocal microscopy; shown are maximum intensity projections from z-stacks through FDC clusters. (Scale bar, 80 μ m.)

over time, and plasmablasts were compared by flow cytometry on days 7 and 13 for both regimens. Significant numbers of GC B cells did not develop following bolus immunization until day 13, and the GCs contracted by day 21 (Fig. 5 *B* and *C*). Exp-inc-vaccinated mice showed germinal center responses over a similar time frame, but GC B-cell numbers escalated dramatically between days 7 and 13, reaching 3.7-fold higher peak levels of GC B cells ($P = 0.040$ for 2-wk exp-inc d13 vs. bolus d13; Fig. 5 *B* and *C*). Notably, exponential dosing led to overall greatly increased cell numbers in lymph nodes at these peak GC time points. Adjuvant-only and antigen-only controls indicated that this germinal center response was largely antigen-specific but dependent on the presence of adjuvant (Fig. 5*C*). Exp-inc vaccination also stimulated a massive expansion of plasma cells on day 13, which was not observed at any time point for traditional bolus immunization ($P < 0.0001$; Fig. 5*D*). B-cell activation in the draining LNs at 24 h after the final injection of the exp-inc dosing regimen was similar to 24-h post-bolus injection (Fig. 5*E*). Thus, an escalating pattern of vaccine dosing amplified the germinal center response and altered B-cell differentiation patterns in the lymph node.

True Continuous Antigen Exposure Elicits Increased Germinal Center and Serum Antibody Responses. Because we experimentally prolonged vaccine dosing through repeated injections, a question that remained was whether similar vaccine results would be obtained in the setting of true continuous antigen exposure. To answer this question, a series of experiments were performed using mini osmotic pumps, nonmechanical delivery devices that

can release a material continuously over a specific period of weeks in vivo when implanted s.c. Mice were immunized with osmotic pumps containing native-like BG505 SOSIP HIV Env trimers (26–28) admixed with an ISCOMs-type adjuvant, and CD4⁺ T-cell, B-cell, and antibody responses were assessed. As shown in Fig. 6*A*, we compared traditional bolus vaccination with SOSIP trimer and ISCOMATRIX to immunizations where osmotic pumps were implanted for release of vaccine over 1 wk or immunizations using pumps releasing vaccine for 2 wk. Motivated by our results that suggest the key feature of the escalating dosing pattern is the availability of antigen at the end of the dosing schedule, we administered a bolus injection at the end of each pump lifespan (days 7 and 14 for the 1 and 2 wk pumps, respectively) to provide a high dose of antigen at the end of the dosing pattern. Animals in each group were boosted with the same regimens after 9 and 20 wk. We evaluated GC B-cell and Tfh cell numbers 4 wk after the final immunization. Sustained immunogen delivery using the osmotic pumps increased the frequency and absolute number of germinal center Tfh cells (CXCR5^{hi} PD-1^{hi}; Fig. 6*B*) and overall Tfh cells (Fig. 6*C*) in the draining lymph nodes. The greatest GC Tfh increase (~three-fold) was observed for pumps providing 2 wk of vaccine release. Total numbers of Tfh cells (CXCR5⁺) measured by flow cytometry were also increased by osmotic pump-based sustained vaccine kinetics, with 2-wk osmotic pumps eliciting the greatest increase in total Tfh numbers compared with bolus immunizations (Fig. 6*C*). Overall numbers of GC B cells were elevated ~threefold by the 2 wk extended dosing osmotic pump regimen (Fig. 6*D*),

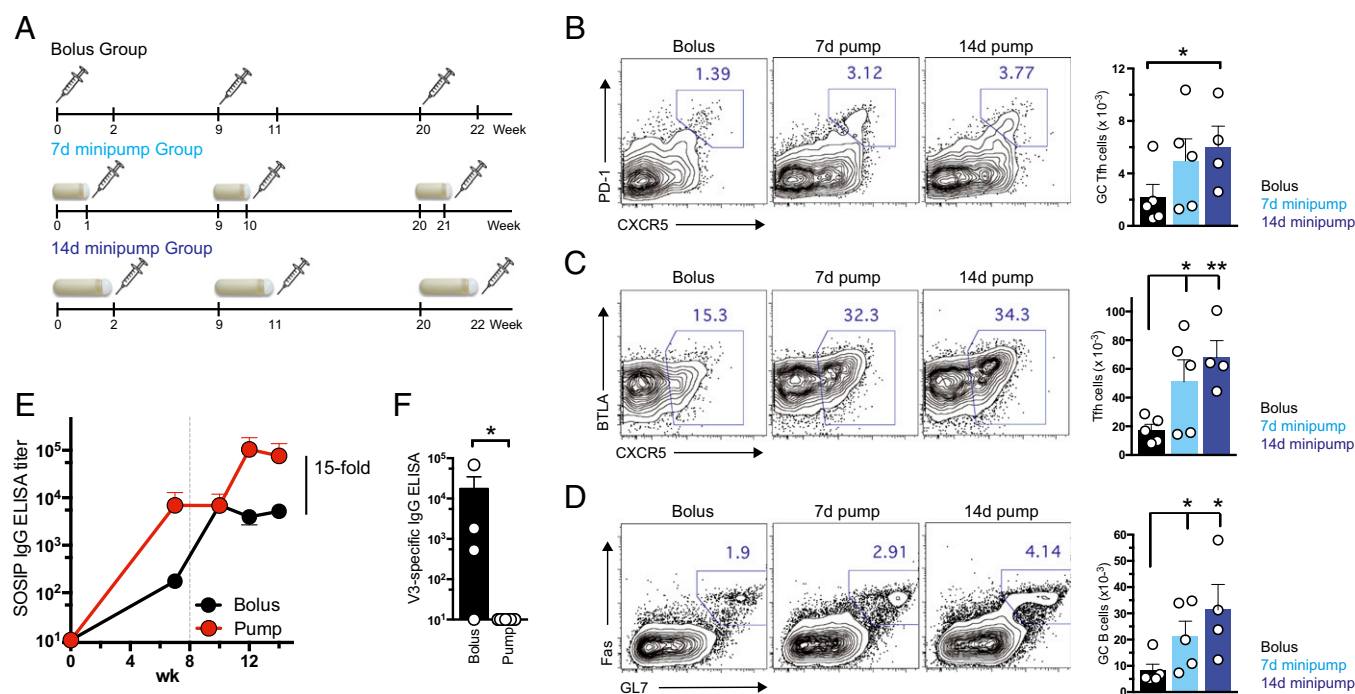


Fig. 6. Continuous vaccine release via osmotic minipumps leads to increased Tfh and GC B cells and amplified antibody responses. (*A–D*) 129S1/SvImJ mice were immunized with 20 μ g HIV-1 Env BG505 SOSIP trimer via conventional bolus injection (Bolus). A second group, 7d minipump, was immunized with 7-d minipumps continuously releasing HIV-1 Env BG505 SOSIP trimers (50 μ g, 7.1 μ g/d), supplemented with 20 μ g BG505 SOSIP trimer via bolus injection at the end of each 7-d pump immunization. A third group, 14d minipump, was immunized with 14-d minipumps continuously releasing HIV-1 Env BG505 SOSIP trimers (100 μ g, 7.1 μ g/d), supplemented with 20 μ g BG505 SOSIP trimer via bolus injection at the end of each 7-d pump immunization. A course of three immunizations was used, paralleling a human vaccine schedule. (*B–D*) Draining LNs were collected at wk 24, 4 wk after the final immunization, and lymphocytes were analyzed by flow cytometry to detect (*B*) GC Tfh cells (CXCR5^{hi}PD-1^{hi}), (*C*) Tfh cells (CXCR5⁺), and (*D*) germinal center B cells (Fas^{hi}GL7^{hi}). Representative flow cytometry plots (*Left*) and cell counts (*Right*) are shown. (*E* and *F*) 129S1/SvImJ mice were immunized with conventional 20 μ g bolus injections of HIV-1 Env BG505 SOSIP trimers (Bolus). A second group was immunized with 14-d minipumps continuously releasing HIV-1 Env BG505 SOSIP trimers (1.4 μ g/d), supplemented with 20 μ g BG505 SOSIP trimer via bolus injection at the end of the 14-d pump immunization (Pump). ISCOMATRIX adjuvant was used in each case. (*E*) Env trimer binding IgG was quantified by ELISA. Dotted line indicates time of second immunization (week 8). (*F*) ELISA for off-target V3 loop antibodies. Data are representative of two independent experiments. * $P < 0.05$; ** $P < 0.01$. Error bars are SEM.

Vaccination and Sample Collection. All procedures used in animal studies were approved by the Committee on Animal Care at the Massachusetts Institute of Technology and the La Jolla Institute for Allergy and Immunology Animal Care Committee and were consistent with local, state, and federal regulations before initiation of this research. Female C57BL/6 mice (8–10 wk old, Jackson Laboratories) were s.c. injected at the base of the tail with indicated doses of gp120 and MPLA in 100 μ L PBS at the specified doses and days. This injection location drains to the inguinal lymph nodes, which were collected postmortem for certain analyses. Alternatively, mice were injected intramuscularly with gp120 formulated in 100 μ g Alum (Adju-Phos, Brenntag Biosector A/S).

For SOSIP trimer immunizations, 6- to 8-wk-old 129S1/SvImJ mice (Jackson Laboratories) were used. Mice were given interscapular bolus immunizations with 20 μ g BG505 SOSIP.664 gp140 in 0.5 Units of ISCOMATRIX (CSL Ltd.). Osmotic pumps containing 100 μ g (2-wk slow release) or 50 μ g (1-wk slow release) BG505 SOSIP.664 gp140 in 0.5 Units of ISCOMATRIX were s.c. implanted in the interscapular region. Blood (from retroorbital or submandibular; 100 μ L) was collected weekly into serum separator tubes (BD Corporation) and centrifuged at $4,000 \times g$ for 10 min at 4 °C. Alternatively, blood was collected in Eppendorf tubes and centrifuged at $16,000 \times g$ for 30 min at 4 °C. Sera extracted from blood samples were stored at –80 °C until ready for analysis.

ELISA. Serum anti-gp120 IgG antibodies were quantified by endpoint ELISA using gp120 as the capture antigen on 96-well Maxisorp microtiter plates (Nunc). Plates were incubated with 0.5 mg/mL poly-L-lysine in PBS for 4 h at room temperature, blocked by 1% BSA in PBS overnight at 4 °C and incubated with 50 nM gp120 in PBS with 1% BSA for 2 h at room temperature. Mouse sera was diluted in PBS with 1% BSA at 1:3,000 or 1:30,000 and incubated for 1.5 h at 25 °C followed by HRP-conjugated goat anti-mouse IgG (1:5,000 in PBS with 1% BSA) for 1 h at 25 °C. Plates were washed four times in between each step with 0.05% tween-20 in PBS. Plates were developed with TMB, stopped with 1M sulfuric acid, and read at 450 and 570 nm using a Tecan M1000 plate reader. Anti-gp120 IgG antibody concentrations were calculated based on ELISA standards using mb12, a monoclonal murine antibody from the NIH AIDS Reagent repository. Analysis was done by subtracting the 570-nm signal from the 450-nm signal, fitting the standard to a four-parameter log-logistic model with the drc package in R, and using that fit to compute antibody concentrations.

Serum anti-BG505 SOSIP.664 gp140 IgG titers were quantified as previously described (39). Briefly, 96-well Maxisorp plates (Thermo Scientific) were coated with 5 μ g/mL D7324 (Aalto Bio Reagents Ltd.) overnight at 4 °C. After blocking with 2% (wt/vol) skim milk, 0.3 μ g/mL C terminus D7324-tagged BG505 SOSIP.664 trimers were added followed by mouse serum and HRP-labeled goat anti-mouse IgG, Fc γ fragment specific (Jackson ImmunoResearch) with washes in between each step. For V3 specific ELISAs, plates were coated overnight at 4 °C with 2 μ g/mL BG505 V3 peptide (TRPNNTNTRKSIRIGPGQAFYATG) in PBS. After blocking, mouse serum was added followed by HRP-labeled goat anti-mouse IgG with washes in between each step. Colorimetric detection was performed using a TMB substrate kit (Thermo Scientific) and stopped with 2N sulfuric acid. Absorbance was read at 450 nm. Endpoint titers were calculated in GraphPad Prism after subtracting the average background optical density (OD) from all values measured at 450 nm.

Flow Cytometry Analysis of Lymph Nodes. Inguinal and brachial lymph nodes were harvested and single-cell suspensions were obtained by passage of the lymph nodes through a 70- μ m filter (BD Biosciences). Cells were washed with PBS and labeled with Live/Dead Aqua (Life Technologies) for 15 min at 25 °C. For B-cell activation and germinal center analysis, samples were treated with anti-CD16/32 (TruStain fcX; BioLegend), followed by staining with anti-CD3e-PerCP-Cy5.5 (BD Biosciences), anti-B220-PE-Cy7 (eBioscience), anti-CD138-PE (BD Biosciences), anti-IgD-APC (eBioscience), anti-GL7-FITC (BD Biosciences), anti-MHCII-AF700 (BioLegend), anti-CD86-V450 (BD Biosciences), and PNA-biotin (VectorLabs) + Streptavidin-APCeF780 (eBioscience). CXCR5 stains were performed as previously described (59). Flow cytometry was carried out on a BD LSR Fortessa or LSR II.

Histology of Lymph Nodes. Inguinal lymph nodes were harvested, embedded in OCT compound, and frozen on dry ice. Frozen tissues were sectioned at 10- μ m thickness, fixed with 4% (vol/vol) paraformaldehyde in PBS, and stained with biotinylated anti-B220 (BioXCell), Streptavidin-APC (BD Biosciences), anti-GL7-FITC (BioLegend), and anti-FITC-AF488 (Jackson ImmunoResearch) for germinal center visualization. Samples were imaged with a PerkinElmer Ultraview Spinning Disk Confocal using a 40 \times oil objective with a Hamamatsu ORCA-ER CCD camera.

Antigen Draining Experiments. Gp120 was labeled with IRDye 800CW-NHS (LI-COR Biosciences) following the manufacturer's instructions. Subsequently, mice were vaccinated with labeled gp120 in the same manner as before according to the dosing profiles in Fig. 4. Mice were killed, and their inguinal lymph nodes were removed. The lymph nodes were digested, and fluorescence was measured using a LI-COR Odyssey CLx Infrared Imaging System (LI-COR Biosciences). Alternatively, mice were vaccinated with intact Phycoerythrin (PE) protein and MPLA as per the aforementioned exp-inc dosing profile or bolus injections and with 10 μ g of BV421 labeled anti-CD21/35 antibody (to label the follicular dendritic cells in vivo) 48 h following the bolus or 48 h following the last exp-inc injection. Sixteen hours after anti-CD21/35 injections, mice were killed, and lymph nodes were extracted and processed to visualize the subnodal distribution of PE relative to FDC in whole intact lymph nodes using the DISCO tissue-clearing method (60). Briefly, lymph nodes were fixed in 4% (vol/vol) paraformaldehyde in PBS for 2 d, washed and cleared using the DISCO solvents, and subsequently imaged using an Olympus Fluoview FV1200 microscope equipped with 30 \times (NA 1.05) objective. The images were then processed and reconstructed using Fiji image analysis software. Z-stacks were acquired for individual FDC clusters. Maximum intensity projections were prepared to show the distribution of antigen across the cluster.

Germinal Center Model Calculations. The computational model accounted for antigen transport/clearance, the germinal center reaction, and antibody production by plasma cells upon vaccinations. The model is expressed in terms of a set of chemical reactions between species, including the four key reactions detailed in Fig. 3B. Parameters used for the model were collected from the literature and are listed in Table S2, with the exception of the plasma cell antibody secretion rate k . This single parameter was fit to reproduce the five IgG measurements made at days 7 and 14 from each dosing strategy. The confidence interval of the best-fit parameter was 1.89×10^6 to 3.16×10^6 . Measurements before the boost injection at day 21 were chosen to fit the parameter because the model does not include memory B cells and, thus, the effect of their reactivation upon boost. Evolution of these reactions in time was determined by computationally solving a set of partial differential equations describing the temporal evolution of these reactions (Table S3) using Matlab; the results were robust with respect to a range of initial conditions.

Statistical Analysis. Error bars are given as SEM of the log-transformed data. Kruskal-Wallis test with Dunn's post hoc test or two-way analysis of variance (ANOVA) with Dunnett's post hoc test were used to account for multiple comparisons in computing confidence intervals. P values were determined by unpaired Mann-Whitney test. Data were plotted and analyzed with GraphPad Prism and R.

ACKNOWLEDGMENTS. We thank the International AIDS Vaccine Initiative and CSL Ltd. for provision of ISCOMATRIX. We thank Sal Butera, The Scripps Research Institute/Center for HIV/AIDS Vaccine Immunology and Immunogen Discovery (CHAVI-ID), for logistical support; the La Jolla Institute animal facility staff for expert assistance with surgeries; and Al Cupo for assistance with HIV Env trimer production. The authors thank the Koch Institute Swanson Biotechnology Center Flow Cytometry and Microscopy core facilities for technical support. This work was supported in part by the Ragon Institute of Massachusetts General Hospital, Massachusetts Institute of Technology (MIT), and Harvard and the Skolkovo-MIT program. Research reported in this publication was supported by the National Institute of Allergy and Infectious Diseases of the National Institutes of Health under Awards UM1AI100663 and AI110657. The content is solely the responsibility of the authors and does not necessarily represent the official views of the National Institutes of Health.

- Bärnighausen T, Bloom DE, Cafiero-Fonseca ET, O'Brien JC (2014) Valuing vaccination. *Proc Natl Acad Sci USA* 111(34):12313–12319.
- Nabel GJ (2013) Designing tomorrow's vaccines. *N Engl J Med* 368(6):551–560.
- Correia BE, et al. (2014) Proof of principle for epitope-focused vaccine design. *Nature* 507(7491):201–206.
- McGuire AT, et al. (2013) Engineering HIV envelope protein to activate germline B cell receptors of broadly neutralizing anti-CD4 binding site antibodies. *J Exp Med* 210(4):655–663.
- Reed SG, Orr MT, Fox CB (2013) Key roles of adjuvants in modern vaccines. *Nat Med* 19(12):1597–1608.
- Rerks-Ngarm S, et al.; MOPH-TAVEG Investigators (2009) Vaccination with ALVAC and AIDSVAX to prevent HIV-1 infection in Thailand. *N Engl J Med* 361(23):2209–2220.
- Bojang KA, et al.; RTS, S Malaria Vaccine Trial Team (2001) Efficacy of RTS,S/AS02 malaria vaccine against *Plasmodium falciparum* infection in semi-immune adult men in The Gambia: a randomised trial. *Lancet* 358(9297):1927–1934.
- Burton DR, Mascola JR (2015) Antibody responses to envelope glycoproteins in HIV-1 infection. *Nat Immunol* 16(6):571–576.
- Crotty S (2014) T follicular helper cell differentiation, function, and roles in disease. *Immunity* 41(4):529–542.
- Ueno H, Bancheau J, Vinuesa CG (2015) Pathophysiology of T follicular helper cells in humans and mice. *Nat Immunol* 16(2):142–152.
- Kasturi SP, et al. (2011) Programming the magnitude and persistence of antibody responses with innate immunity. *Nature* 470(7335):543–547.

12. Moon JJ, et al. (2012) Enhancing humoral responses to a malaria antigen with nanoparticle vaccines that expand Tfh cells and promote germinal center induction. *Proc Natl Acad Sci USA* 109(4):1080–1085.
13. Baumjohann D, et al. (2013) Persistent antigen and germinal center B cells sustain T follicular helper cell responses and phenotype. *Immunity* 38(3):596–605.
14. Vitoria GD, et al. (2010) Germinal center dynamics revealed by multiphoton microscopy with a photoactivatable fluorescent reporter. *Cell* 143(4):592–605.
15. Butler NS, et al. (2011) Therapeutic blockade of PD-L1 and LAG-3 rapidly clears established blood-stage Plasmodium infection. *Nat Immunol* 13(2):188–195.
16. Francica JR, et al.; NISC Comparative Sequencing Program (2015) Analysis of immunoglobulin transcripts and hypermutation following SHIV(AD8) infection and protein-plus-adjuvant immunization. *Nat Commun* 6:6565.
17. Lin WH, Kouyos RD, Adams RJ, Grenfell BT, Griffin DE (2012) Prolonged persistence of measles virus RNA is characteristic of primary infection dynamics. *Proc Natl Acad Sci USA* 109(37):14989–14994.
18. Simon ID, Publicover J, Rose JK (2007) Replication and propagation of attenuated vesicular stomatitis virus vectors in vivo: Vector spread correlates with induction of immune responses and persistence of genomic RNA. *J Virol* 81(4):2078–2082.
19. Luker KE, Hutchens M, Schultz T, Pekosz A, Luker GD (2005) Bioluminescence imaging of vaccinia virus: Effects of interferon on viral replication and spread. *Virology* 341(2):284–300.
20. Pape KA, Catron DM, Itano AA, Jenkins MK (2007) The humoral immune response is initiated in lymph nodes by B cells that acquire soluble antigen directly in the follicles. *Immunity* 26(4):491–502.
21. Gupta RK (1998) Aluminum compounds as vaccine adjuvants. *Adv Drug Deliv Rev* 32(3):155–172.
22. Dupuis M, McDonald DM, Ott G (1999) Distribution of adjuvant MF59 and antigen gD2 after intramuscular injection in mice. *Vaccine* 18(5-6):434–439.
23. Hutchison S, et al. (2012) Antigen depot is not required for alum adjuvanticity. *FASEB J* 26(3):1272–1279.
24. Wang S, et al. (2015) Manipulating the selection forces during affinity maturation to generate cross-reactive HIV antibodies. *Cell* 160(4):785–797.
25. Mata-Fink J, et al. (2013) Rapid conformational epitope mapping of anti-gp120 antibodies with a designed mutant panel displayed on yeast. *J Mol Biol* 425(2):444–456.
26. Lyumkis D, et al. (2013) Cryo-EM structure of a fully glycosylated soluble cleaved HIV-1 envelope trimer. *Science* 342(6165):1484–1490.
27. Julien JP, et al. (2013) Crystal structure of a soluble cleaved HIV-1 envelope trimer. *Science* 342(6165):1477–1483.
28. Sanders RV, et al. (2013) A next-generation cleaved, soluble HIV-1 Env trimer, BG505 SOSIP.664 gp140, expresses multiple epitopes for broadly neutralizing but not non-neutralizing antibodies. *PLoS Pathog* 9(9):e1003618.
29. Garçon N, Van Mechelen M (2011) Recent clinical experience with vaccines using MPL and QS-21-containing adjuvant systems. *Expert Rev Vaccines* 10(4):471–486.
30. Kool M, Fierens K, Lambrecht BN (2012) Alum adjuvant: Some of the tricks of the oldest adjuvant. *J Med Microbiol* 61(Pt 7):927–934.
31. Carroll MC (1998) The role of complement and complement receptors in induction and regulation of immunity. *Annu Rev Immunol* 16:545–568.
32. Boes M (2000) Role of natural and immune IgM antibodies in immune responses. *Mol Immunol* 37(18):1141–1149.
33. Tew JG, Mandel TE (1979) Prolonged antigen half-life in the lymphoid follicles of specifically immunized mice. *Immunology* 37(1):69–76.
34. Song H, Nie X, Basu S, Cerny J (1998) Antibody feedback and somatic mutation in B cells: Regulation of mutation by immune complexes with IgG antibody. *Immunol Rev* 162:211–218.
35. Szakal AK, Kosco MH, Tew JG (1988) FDC-icosome mediated antigen delivery to germinal center B cells, antigen processing and presentation to T cells. *Adv Exp Med Biol* 237:197–202.
36. Dixit NM, Srivastava P, Vishnoi NK (2012) A finite population model of molecular evolution: Theory and computation. *J Comput Biol* 19(10):1176–1202.
37. Corti D, et al. (2011) A neutralizing antibody selected from plasma cells that binds to group 1 and group 2 influenza A hemagglutinins. *Science* 333(6044):850–856.
38. Sanders RW, et al. (2015) HIV-1 VACCINES. HIV-1 neutralizing antibodies induced by native-like envelope trimers. *Science* 349(6244):aac4223.
39. Hu JK, et al. (2015) Murine antibody responses to cleaved soluble HIV-1 envelope trimers are highly restricted in specificity. *J Virol* 89(20):10383–10398.
40. Amanna IJ, Slifka MK (2011) Contributions of humoral and cellular immunity to vaccine-induced protection in humans. *Virology* 411(2):206–215.
41. Cubas RA, et al. (2013) Inadequate T follicular cell help impairs B cell immunity during HIV infection. *Nat Med* 19(4):494–499.
42. Yamamoto T, et al. (2015) Quality and quantity of TFH cells are critical for broad antibody development in SHIVAD8 infection. *Sci Transl Med* 7(298):298ra120.
43. Locci M, et al.; International AIDS Vaccine Initiative Protocol C Principal Investigators (2013) Human circulating PD-1+CXCR3-CXCR5+ memory Tfh cells are highly functional and correlate with broadly neutralizing HIV antibody responses. *Immunity* 39(4):758–769.
44. Dosenovic P, et al. (2015) Immunization for HIV-1 broadly neutralizing antibodies in human Ig knockin mice. *Cell* 161(7):1505–1515.
45. Haynes BF, Kelsoe G, Harrison SC, Kepler TB (2012) B-cell-lineage immunogen design in vaccine development with HIV-1 as a case study. *Nat Biotechnol* 30(5):423–433.
46. Moyer TJ, Zmolek AC, Irvine DJ (2016) Beyond antigens and adjuvants: Formulating future vaccines. *J Clin Invest* 126(3):799–808.
47. Kemp JM, et al. (2002) Continuous antigen delivery from controlled release implants induces significant and anamnestic immune responses. *Vaccine* 20(7-8):1089–1098.
48. Spiers ID, Eyles JE, Baillie LW, Williamson ED, Alpar HO (2000) Biodegradable micro-particles with different release profiles: Effect on the immune response after a single administration via intranasal and intramuscular routes. *J Pharm Pharmacol* 52(10):1195–1201.
49. Thomasin C, Corradin G, Men Y, Merkle H, Gander B (1996) Tetanus toxoid and synthetic malaria antigen containing poly (lactide)/poly (lactide-co-glycolide) microspheres: Importance of polymer degradation and antigen release for immune response. *J Control Release* 41(1-2):131–145.
50. Preis I, Langer RS (1979) A single-step immunization by sustained antigen release. *J Immunol Methods* 28(1-2):193–197.
51. Johansen P, et al. (2008) Antigen kinetics determines immune reactivity. *Proc Natl Acad Sci USA* 105(13):5189–5194.
52. Demuth PC, Garcia-Beltran WF, Ai-Ling ML, Hammond PT, Irvine DJ (2013) Composite dissolving microneedles for coordinated control of antigen and adjuvant delivery kinetics in transcutaneous vaccination. *Adv Funct Mater* 23(2):161–172.
53. Pekarek KJ, Jacob JS, Mathiowitz E (1994) Double-walled polymer microspheres for controlled drug release. *Nature* 367(6460):258–260.
54. Prescott JH, et al. (2006) Chronic, programmed polypeptide delivery from an implanted, multireservoir microchip device. *Nat Biotechnol* 24(4):437–438.
55. Xia Y, Pack DW (2014) Pulsatile protein release from monodisperse liquid-core microcapsules of controllable shell thickness. *Pharm Res* 31(11):3201–3210.
56. Ford Versypt AN, Pack DW, Braatz RD (2013) Mathematical modeling of drug delivery from autocatalytically degradable PLGA microspheres—A review. *J Control Release* 165(1):29–37.
57. Soppimath KS, Aminabhavi TM, Kulkarni AR, Rudzinski WE (2001) Biodegradable polymeric nanoparticles as drug delivery devices. *J Control Release* 70(1-2):1–20.
58. Chung NP, et al. (2014) Stable 293 T and CHO cell lines expressing cleaved, stable HIV-1 envelope glycoprotein trimers for structural and vaccine studies. *Retrovirology* 11:33.
59. Choi YS, et al. (2011) ICOS receptor instructs T follicular helper cell versus effector cell differentiation via induction of the transcriptional repressor Bcl6. *Immunity* 34(6):932–946.
60. Ertürk A, et al. (2012) Three-dimensional imaging of solvent-cleared organs using 3DISCO. *Nat Protoc* 7(11):1983–1995.
61. Mandel TE, Phipps RP, Abbot A, Tew JG (1980) The follicular dendritic cell: Long term antigen retention during immunity. *Immunol Rev* 53:29–59.
62. Mankarious S, et al. (1988) The half-lives of IgG subclasses and specific antibodies in patients with primary immunodeficiency who are receiving intravenously administered immunoglobulin. *J Lab Clin Med* 112(5):634–640.
63. Kepler TB, Perelson AS (1993) Cyclic re-entry of germinal center B cells and the efficiency of affinity maturation. *Immunol Today* 14(8):412–415.
64. Meyer-Hermann M, et al. (2012) A theory of germinal center B cell selection, division, and exit. *Cell Reports* 2(1):162–174.
65. Meyer-Hermann ME, Maini PK, Iber D (2006) An analysis of B cell selection mechanisms in germinal centers. *Math Med Biol* 23(3):255–277.
66. Zhang J, Shakhnovich EI (2010) Optimality of mutation and selection in germinal centers. *PLOS Comput Biol* 6(6):e1000800.
67. Proulx ST, et al. (2007) MRI and quantification of draining lymph node function in inflammatory arthritis. *Ann N Y Acad Sci* 1117:106–123.
68. Townsley-Fuchs J, et al. (1996) Human immunodeficiency virus-1 (HIV-1) gp120 super-antigen-binding serum antibodies. A host factor in homosexual HIV-1 transmission. *J Clin Invest* 98(8):1794–1801.